

ACCEPTED MANUSCRIPT

In-vivo estimation of anisotropic mechanical properties of the gastrocnemius during functional loading with MR elastography

To cite this article before publication: Daniel R Smith *et al* 2023 *Phys. Med. Biol.* in press <https://doi.org/10.1088/1361-6560/acb482>

Manuscript version: Accepted Manuscript

Accepted Manuscript is “the version of the article accepted for publication including all changes made as a result of the peer review process, and which may also include the addition to the article by IOP Publishing of a header, an article ID, a cover sheet and/or an ‘Accepted Manuscript’ watermark, but excluding any other editing, typesetting or other changes made by IOP Publishing and/or its licensors”

This Accepted Manuscript is © 2023 Institute of Physics and Engineering in Medicine.

During the embargo period (the 12 month period from the publication of the Version of Record of this article), the Accepted Manuscript is fully protected by copyright and cannot be reused or reposted elsewhere.

As the Version of Record of this article is going to be / has been published on a subscription basis, this Accepted Manuscript is available for reuse under a CC BY-NC-ND 3.0 licence after the 12 month embargo period.

After the embargo period, everyone is permitted to use copy and redistribute this article for non-commercial purposes only, provided that they adhere to all the terms of the licence <https://creativecommons.org/licenses/by-nc-nd/3.0>

Although reasonable endeavours have been taken to obtain all necessary permissions from third parties to include their copyrighted content within this article, their full citation and copyright line may not be present in this Accepted Manuscript version. Before using any content from this article, please refer to the Version of Record on IOPscience once published for full citation and copyright details, as permissions will likely be required. All third party content is fully copyright protected, unless specifically stated otherwise in the figure caption in the Version of Record.

View the [article online](#) for updates and enhancements.

1
2
3 1 **TITLE: *In-Vivo* Estimation of Anisotropic Mechanical Properties of the Gastrocnemius during**
4 **Functional Loading with MR Elastography**

5 2
6
7 3 Authors: Daniel R. Smith^{1,2,3}, Diego A. Caban-Rivera¹, L. Tyler Williams¹, Elijah E.W. Van Houten⁴,
8
9 4 Phil V. Bayly⁵, Keith D. Paulsen^{6,7}, Matthew D.J. McGarry⁶, Curtis L. Johnson¹

10 5 1: Department of Biomedical Engineering, University of Delaware, Newark DE, 19711

11 6 2: Department of Orthopaedics, Emory University School of Medicine, Atlanta GA, 30307

12 7 3: Emory Sports Performance and Research Center, Flowery Branch GA, 30542

13 8 4: Université de Sherbrooke, Sherbrooke, QC, Canada J1K 2R1

14 9 5: Department of Mechanical Engineering and Materials Science, Washington University in St.
15
16 10 Louis, St. Louis MO

17 11 6: Thayer School of Engineering, Dartmouth College, Hanover NH, 03755

18 12 7: Dartmouth-Hitchcock Medical Center, Lebanon NH, 03756

19 13

20 14 **Correspondence To:**

21 15 Curtis L. Johnson, PhD

22 16 150 Academy St.

23 17 Newark, DE 19716

24 18 clj@udel.edu

25 19

26 20 **Approximate Word Count: 3500**

27 21

1
2
3 **1 Abstract**

4 **2 Objective:** *In-vivo* imaging assessments of skeletal muscle structure and function allow for
5
6 longitudinal quantification of tissue health. Magnetic resonance elastography (MRE) non-
7
8 invasively quantifies tissue mechanical properties, allowing for evaluation of skeletal muscle
9
10 biomechanics in response to loading, creating a better understanding of muscle functional
11
12 health.

13 **3 Approach:** In this study, we analyze the anisotropic mechanical response of calf muscles using
14
15 MRE with a transversely isotropic, nonlinear inversion algorithm (TI-NLI) to investigate the role
16
17 of muscle fiber stiffening under load. We estimate anisotropic material parameters including
18
19 fiber shear stiffness (μ_1), substrate shear stiffness (μ_2), shear anisotropy (ϕ), and tensile
20
21 anisotropy (ζ) of the gastrocnemius muscle in response to both passive and active tension.
22
23

24 **4 Main Results:** In passive tension, we found a significant increase in μ_1 , ϕ , and ζ with increasing
25
26 muscle length. While in active tension, we observed increasing μ_2 and decreasing ϕ and ζ
27
28 during active dorsiflexion and plantarflexion – indicating less anisotropy – with greater effects
29
30 when the muscles act as agonist.

31 **5 Significance:** The study demonstrates the ability of this anisotropic MRE method to capture the
32
33 multifaceted mechanical response of skeletal muscle to tissue loading from muscle lengthening
34
35 and contraction.

36 **6 Keywords:** Magnetic Resonance Elastography, Skeletal Muscle, Stiffness, Tension,
37
38 Gastrocnemius
39
40
41
42
43
44
45
46
47
48
49
50
51
52
53
54
55
56
57
58
59
60

1 1. Introduction

2 Non-invasive evaluation of skeletal muscle health *in-vivo* allows for longitudinal
3 assessments of tissue structure and function. Primary assessment tools include measurement
4 of muscle activation through surface electromyography (sEMG) [1–3], and imaging of tissue
5 structure with ultrasound imaging [4–6] and magnetic resonance imaging (MRI) [7,8]. These
6 techniques each have their advantages, with sEMG and ultrasound imaging providing high
7 temporal resolution during muscle activation, while MRI provides a large field-of-view (FOV) to
8 better investigate multiple muscles and their interactions simultaneously. An additional benefit
9 of MRI is the ability to more comprehensively examine the complex structure of skeletal muscle
10 by combining standard MRI contrasts, such as T1-weighted [9–11] and T2-weighted [12–14]
11 imaging, with quantitative contrasts sensitive to tissue biophysics, such as diffusion tensor
12 imaging (DTI) [15–17] and MR spectroscopy [18,19].

13 One such MRI modality is magnetic resonance elastography (MRE), which is a phase-
14 contrast technique that measures propagating time-harmonic shear waves to probe the
15 mechanical properties of tissues and has been successfully used to analyze the health of other
16 human organs [20–23]. In skeletal muscle, MRE has shown to capture changes in tissue
17 mechanical properties reflecting muscle microstructure due to aging [24,25], exercise [26,27],
18 and pathology, including Duchenne muscle dystrophy [28–30]. MRE has also shown to reflect
19 muscle activation through changes in the apparent mechanical stiffness of the tissue. In
20 particular, Zonnino, et al. [31] quantified the effects of variable isometric contraction on MRE
21 estimates in the human forearm, as well as how changing muscle length affected the responses
22 of those muscles. Additionally, Schrank, et al. [32] used a real-time MRE method to quantify

1 parameter changes in calf muscles during isometric contraction loading conditions. In these
2 examples, muscles appeared stiffer during contraction, indicating an avenue to better
3 understand muscle force output.

4 While previous studies have demonstrated the potential of MRE for characterizing
5 skeletal muscle, they have largely employed isotropic material models when estimating tissue
6 mechanical properties, which are then susceptible to inaccuracies given the fibrous
7 composition of muscle that leads to anisotropic mechanical behavior [33,34]. Several recent
8 MRE studies of skeletal muscle have attempted to incorporate mechanical anisotropy, including
9 works by Green, et al. [35], Guo, et al. [36], and Babaei, et al. [37]. These studies each modeled
10 muscle as an incompressible, transversely isotropic tissue with two anisotropic shear
11 parameters defining the tissue response to shear deformations parallel and perpendicular to
12 the muscle fibers. Fiber stretching, a critical component of the mechanical response of muscle
13 during contraction, cannot be represented by two shear parameters alone, and instead requires
14 an additional parameter to capture the tensile mechanical response. Recently, a nearly
15 incompressible, transversely isotropic (NITI) material model, which incorporates three
16 parameters to describe the tissue – substrate shear stiffness, shear anisotropy, and tensile
17 anisotropy – has shown promise in modeling both the shear and tensile components of
18 anisotropy in fibrous human tissue when combined with MRE displacement data [38–42].
19 Through estimation of the three independent mechanical property parameters, the NITI
20 material model provides an effective framework from which to quantify the mechanical
21 response of skeletal muscle as it is functionally activated.

1
2
3 1 Most studies analyzing the link between measurements of anisotropic mechanical
4
5 2 properties of skeletal muscle and tissue structure and function have utilized *ex-vivo* techniques
6
7 3 and have shown significant variations in tissue mechanical response during both passive
8
9 4 stretching and active contraction [43,44]. These prior works have characterized muscle force
10
11 5 production and transmission in both the axial and lateral directions [45–47], with greater axial
12
13 6 loading in the direction of the muscle fibers occurring during passive stretching, while active
14
15 7 contraction produces higher forces in the lateral direction [48,49]. Capturing these variations in
16
17 8 muscle mechanics *in-vivo* would allow for more accurate assessments of skeletal muscle
18
19 9 functional responses that incorporate the entire muscle volume, and other muscles and bone
20
21 10 that make up the lower leg. Additionally, it would establish MRE as sensitive to tissue structure
22
23 11 and function to allow for the assessment of longitudinal effects of injury and pathology in
24
25 12 individual subjects.

26
27 13 Therefore, the purpose of this study is use MRE to capture anisotropic mechanical
28
29 14 behavior in skeletal muscle *in-vivo* consistent to previous *ex-vivo* studies. To test this, we
30
31 15 estimated the anisotropic mechanical properties of skeletal muscle using the recently
32
33 16 developed transversely isotropic, nonlinear inversion algorithm (TI-NLI) that incorporates wave
34
35 17 motion fields from MRE with fiber orientation data acquired with diffusion tensor imaging (DTI)
36
37 18 [50,51]. We performed two experiments to probe the mechanical reaction of skeletal muscle:
38
39 19 the first to investigate passive contraction through muscle stretching, and the second to
40
41 20 explore the mechanical variations caused by active isometric contraction.
42
43
44
45
46
47
48
49
50
51
52
53
54
55
56
57
58
59
60

1
2
3 **1 2. Methods**
4

5
6 **2 2.1 Experimental Setup**
7

8 Eight healthy young adult subjects (4/4 M/F; ages 23-26) completed the study approved
9
10 by our Institutional Review Board. All participants were imaged in a Siemens 3T Prisma MRI
11
12 scanner. Each subject was positioned supine, feet first in the bore with legs draped over an
13
14 adjustable support as shown in Figure 1. Two RF receiver coils were wrapped around the calf
15
16 with two custom-made passive drivers to generate the necessary shear waves for MRE in
17
18 conjunction with the Resoundant pneumatic actuation system. For Experiment 1, the right
19
20 ankle of each subject was placed in a custom brace to limit range of motion while the height of
21
22 the knee was adjusted to achieve three different angles: 105°, 135°, and 165°. For Experiment
23
24 2, the right foot of each subject was positioned on a pedal device. Individuals were instructed
25
26 to press and hold down one side of the footplate to compress fully one of the plastic springs, as
27
28 illustrated in Figure 1B, for the duration of each MRE scan. This positioning induced isometric
29
30 dorsi- or plantar-flexion depending on which spring the subject compressed. Subjects practiced
31
32 these movements prior to scanning to acclimate themselves to the force required to minimize
33
34 variability between participants and acquisitions.
35
36
37
38
39
40
41
42
43
44
45
46
47
48
49
50
51
52
53
54
55
56
57
58
59
60

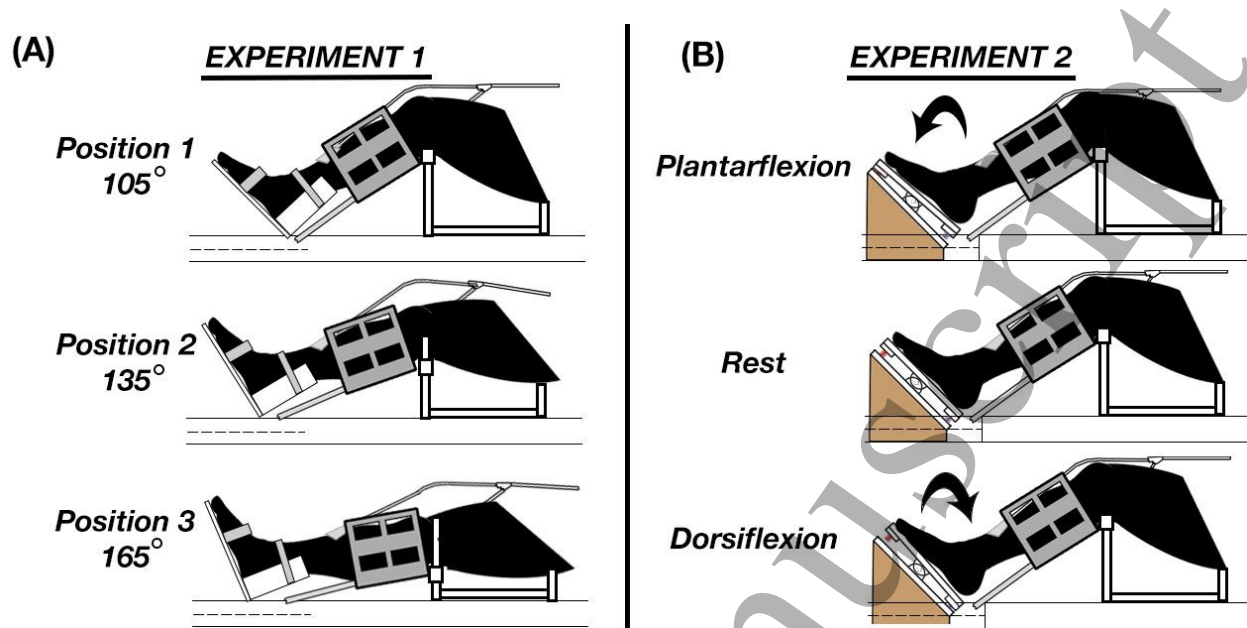


Figure 1: (A) Experiment 1 entailed placing the subject's foot in a custom ankle brace to maintain a constant ankle angle while the angle of subject's knee was altered through raising or lowering the leg support. (B) Experiment 2 replaces the ankle brace with a pedal-like device which induced isometric contraction when the subject pushed against one of the two springs during dorsi- or plantar-flexion, while the leg was supported at a constant knee angle.

2.2 Imaging Protocol

MRE data was collected using an echo-planar imaging (EPI) sequence with the following parameters: $2 \times 2 \times 3 \text{ mm}^3$ voxel size; FOV = $160 \times 160 \text{ mm}$; 80×80 matrix; 20 slices with 3 mm thickness; repetition time (TR)/ echo time (TE) = 2400/59 ms; vibration frequency = 50 Hz; 4 phase offsets; dual gradient polarity; total acquisition time = 65 sec. Thicker slices were used to increase signal-to-noise ratio, and were positioned axially where anatomical features and mechanical properties are assumed to vary more slowly along the leg. We also acquired a diffusion tensor imaging (DTI) scan with resolution and FOV matched to the MRE data with TR/TE = 2200/69 ms, $b = 400 \text{ s/mm}^2$ and 30 directions, as well as a T1-weighted scan with the following parameters: $1.25 \times 1.25 \times 3 \text{ mm}^3$ voxel size; FOV = $160 \times 160 \text{ mm}$; 128×128 matrix; 20 slices; TR/TE = 2200/11 ms;

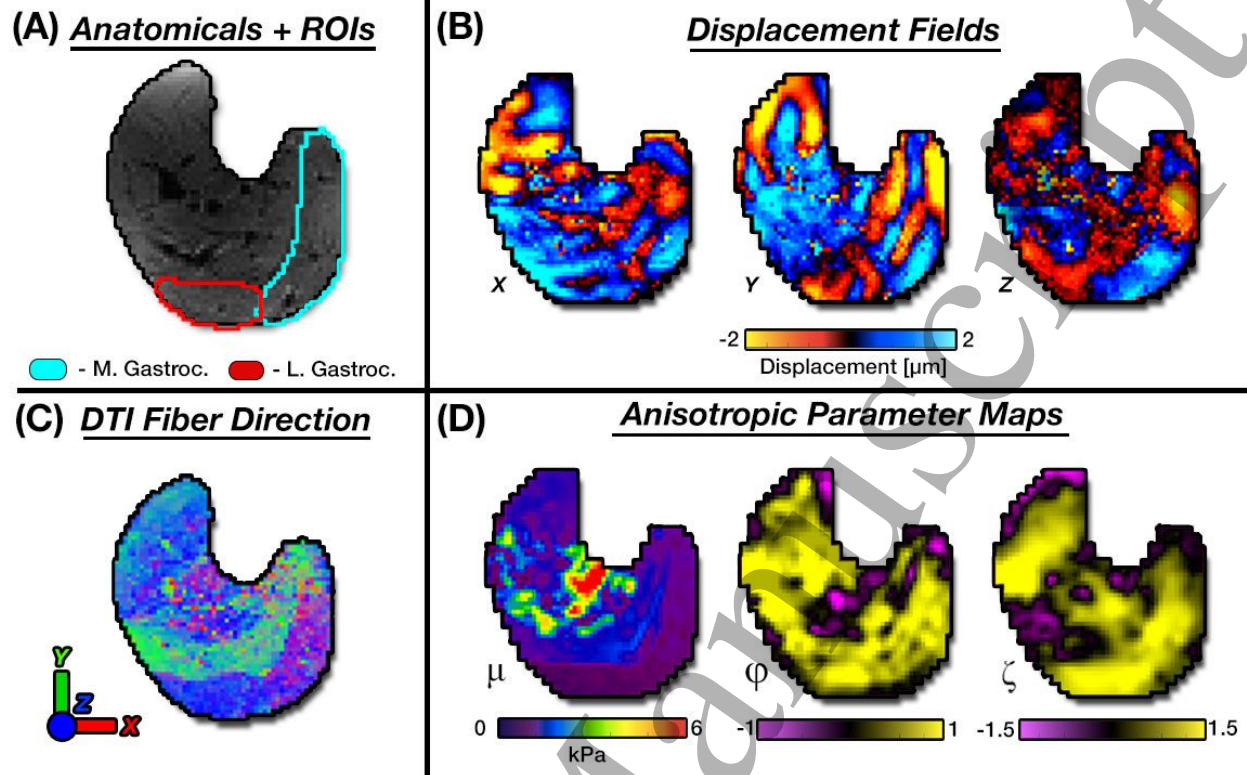


Figure 2: (A) Two primary muscles, medial and lateral heads of the gastrocnemius, were investigated to determine anisotropic material parameters. Three material property parameters were estimated by combining (B) MRE displacement fields with (C) DTI fiber directions. The anisotropic parameters included (D) substrate shear stiffness (μ), shear anisotropy (ϕ), and tensile anisotropy (ζ).

Each subject completed both Experiment 1 and Experiment 2 within the same scanning session. Experiment 1 consisted of a set of image acquisitions at each of three knee angles (105°, 135°, and 165°). At each position, we collected three repeated MRE scans, one DTI scan, and one T1-weighted anatomical scan. Experiment 2 consisted of three repeated MRE acquisitions during each contraction condition – dorsi-flexion, plantar-flexion, and rest – for a total of nine MRE scans. Additionally, we acquired one DTI scan and one T1-weighted anatomical scan as in Experiment 1. All imaging volumes were manually aligned to be axial to the leg for different leg positions in both experiments.

2.3 Data Processing

1 Diffusion data was processed with the FMRIB's Diffusion Toolbox (FDT) from FMRIB's
2 Software Library (FSL) [52]. We then used FMRIB's Linear Image Registration Tool (FLIRT) to
3 register the diffusion-weighted images with MRE image space using the diffusion gradient
4 directions for each image rotated according to the registration. From there, fractional
5 anisotropy and the first eigenvector (V_1) were calculated using FDT.

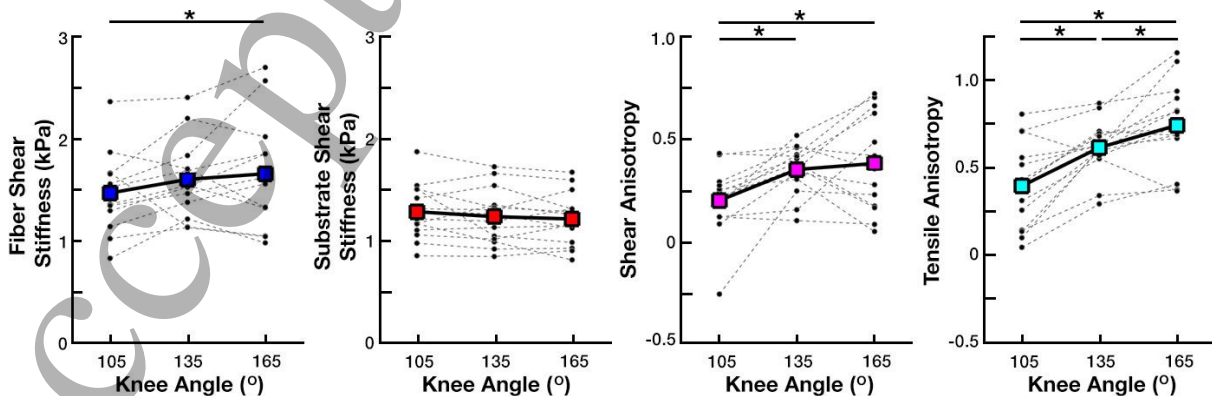
6 Wave motion fields were calculated from MRE data after subtraction to remove background
7 phase, phase unwrapping with FSL PRELUDE [53], and temporal Fourier filtering to isolate the
8 harmonic motion of interest. We then used a transversely isotropic, non-linear inversion
9 algorithm (TI-NLI) to estimate anisotropic material parameters based on the acquired wave
10 motion fields and the primary eigenvector from DTI, the assumed fiber direction [50,51], as
11 shown in Figure 2. TI-NLI is an iterative, finite element-based inversion that estimates spatial
12 maps of the three material property parameters used to describe a NITI model: substrate shear
13 modulus, G_2 , shear anisotropy, $\phi = |G_1|/|G_2| - 1$, and tensile anisotropy, $\zeta = |E_1|/|E_2| - 1$,
14 where G and E are defined as a material shear and tensile moduli respectively. Subscript 1
15 denotes a property parallel to the direction of the fiber, or normal to the plane of isotropy,
16 while a subscript 2 denotes a property perpendicular to the fiber direction, or in the plane of
17 isotropy. The substrate shear modulus is defined by the equation: $G_2 = G'_2 + iG''_2$, where G'_2 is
18 the substrate storage modulus, and G''_2 is the substrate loss modulus. Here we calculate the
19 substrate shear stiffness as $\mu_2 = \frac{2|G_2|^2}{G'_2 + |G_2|}$ which describes the square of the wave speed
20 perpendicular to the fibers. We also considered the shear stiffness parallel to the fibers as $\mu_1 =$
21 $\mu_2(1 + \phi)$. We note that the parameters estimated in this study are "effective" mechanical

1 properties due to the nonlinear acoustoelastic effects of the pre-strain fields on the skeletal
2 muscle [54].

3 We estimated the average anisotropic properties in individual calf muscles, specifically the
4 medial and lateral heads of the gastrocnemius, which were manually traced from anatomical
5 images. Within TI-NLI, we applied soft prior regularization using these generated volumes as *a*
6 *priori* spatial information to stabilize the estimation of properties [55]. To analyze differences in
7 muscle parameters between contraction states, we applied a linear mixed model with variables
8 of muscle, subject, and position as fit parameters for Experiment 1, and a one-way ANOVA with
9 repeated measures within subject and muscle with relationships between a post-hoc Tukey test
10 for Experiment 2.

15 3. Results

16 3.1 Experiment 1 – Passive Muscle Lengthening



17

1 *Figure 3: Results from Experiment 1 comparing the effects of increasing muscle length with*
2 *knee angle on fiber shear stiffness, substrate shear stiffness, shear anisotropy, and tensile*
3 *anisotropy (left to right) in both heads of the gastrocnemius muscle. Statistically significant*
4 *differences are denoted by *.*

5 Figure 3 displays results from Experiment 1 and shows changes in the anisotropic
6 material parameters in the gastrocnemii when placed in the three knee positions: 105°, 135°,
7 and 165°. Associated descriptive statistics are summarized in Table 1. We found increases in μ_1 ,
8 ϕ , and ζ as knee angle increases (each $p < 0.05$), while μ_2 stayed relatively stable. Using data
9 from both muscles individually, μ_1 increased by approximately 7.6% overall, from 1.66 kPa to
10 1.79 kPa, between the initial and final position ($p = 0.061$). ϕ , however, increased 7.6%
11 between a knee angle of 105° and 135° and 1.8% between a knee angle of 135° and 165°, for a
12 total increase of 9.5% from 0.30 to 0.33 ($p < 0.05$). ζ exhibited similar increases the three knee
13 positions – 38% between a knee angle of 105° and 135° and 33% between a knee angle of 135°
14 and 165° for an overall increase of 84% ($p < 0.05$).

15
16 Table 1: Average and standard deviations of four mechanical property parameters at the three knee
17 angles measured during Experiment 1.

	μ_1 (kPa)	μ_2 (kPa)	ϕ	ζ
105°	1.49 ± 0.41	1.28 ± 0.27	0.20 ± 0.17	0.40 ± 0.24
135°	1.62 ± 0.40	1.23 ± 0.27	0.35 ± 0.12	0.62 ± 0.16
165°	1.67 ± 0.57	1.21 ± 0.26	0.38 ± 0.24	0.74 ± 0.25

3.2 Active Muscle Contraction

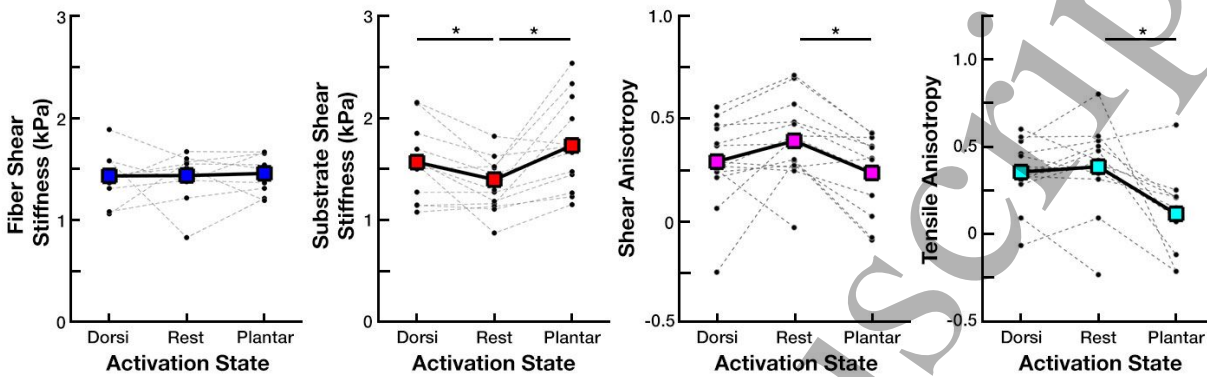


Figure 4: Results from Experiment 2 comparing the effects of isometric contraction on fiber shear stiffness, substrate shear stiffness, shear anisotropy, and tensile anisotropy (left to right) in both heads of the gastrocnemius muscle. Statistically significant differences are denoted by *.

Figure 4 highlights the anisotropic parameter estimates of gastrocnemius during isometric contraction in dorsi-flexion and plantar-flexion relative to rest from Experiment 2. Here, the parameters – μ_2 , ϕ , and ζ – exhibited significant changes between the contraction states ($p < 0.05$), while μ_1 was relatively stable. From the rest condition, μ_2 increased from 1.39 kPa to 1.56 kPa during dorsiflexion ($p < 0.05$) and to 1.73 kPa during plantarflexion ($p < 0.05$), increases of 20% and 13%, respectively. ϕ and ζ had opposite responses, instead showing non-significant decreases from 0.13 to 0.03 (34.6%; $p = 0.106$) and 0.39 to 0.36 (6.9%; $p = 0.72$) during dorsiflexion, respectively, and significant decreases from 0.13 to -0.02 (66.7%; $p < 0.05$) and 0.39 to 0.12 (67.5%; $p < 0.05$) during plantarflexion.

Table 2: Average and standard deviations of four mechanical property parameters at the three different active contraction states measured during Experiment 2.

	μ_1 (kPa)	μ_2 (kPa)	ϕ	ζ
Dorsiflexion	1.43 ± 0.29	1.56 ± 0.36	0.03 ± 0.20	0.36 ± 0.18
Rest	1.43 ± 0.38	1.39 ± 0.30	0.13 ± 0.19	0.39 ± 0.24

Plantarflexion	1.45 ± 0.19	1.73 ± 0.45	-0.02 ± 0.19	0.12 ± 0.23
-----------------------	-----------------	-----------------	------------------	-----------------

1

4. Discussion

In this study, we used MRE to capture the mechanical response occurring in skeletal muscle during isometric contraction and passive lengthening, specifically captured variations in anisotropic mechanical properties of the medial and lateral heads of the gastrocnemius muscle. Most *in-vivo* evaluations of anisotropic mechanical properties of skeletal muscle quantify the resting state shear stiffness and shear anisotropy. In this study, measurements of shear stiffness and shear anisotropy were relatively similar to results from previous reports in the MRE literature with similar vibration frequencies ($\mu_1 = 1.26 - 1.32$ kPa, $\mu_2 = 1.53 - 2.00$ kPa, and $\phi = 0.18 - 0.59$) [35–37]. The repeatability of the estimated shear moduli were within the range of previous MRE studies, with the coefficient of variation, defined as $\frac{Mean}{St.Dev.}$, for the repeated measurements of a single subject averaging 5.0% in experiment 1 and 10.9% in experiment 2 [42,56]. None of the prior published studies reported ζ as a material parameter; hence, comparisons were not possible with the data presented here. In previous studies, MRE-measurements of calf muscles have utilized large knee angles with a nearly-straight leg and a non-flexed ankle, most similarly to our Position 3 at 165° knee angle during Experiment 1. The TI-NLI employed in this study has been demonstrated to accurately recover μ , ϕ and ζ images using realistic simulated data which supports the accuracy of our measurements. [50,57].

In Experiment 1, we showed the degree of anisotropic parameter change during alterations in passive tension on a muscle through changes in muscle length. The gastrocnemius is the only dual-joint muscle in the calf, meaning it crosses both knee and ankle joints.

1
2
3 1 Therefore, by limiting the motion of the ankle, we can alter the length and pennation angle of
4
5 2 the gastrocnemius by changing knee angle and increase the length of the sarcomeres within the
6
7 3 muscle fibers [58,59]. Previous literature has shown that this increases in muscle length also
8
9 4 increases the applied load on the muscle fibers [60–62]. This outcome is reflected in results
10
11 5 from Experiment 1, where μ_1 , the shear stiffness in planes parallel to the fiber direction,
12
13 6 increased with increasing knee angle. One of the primary drivers of this increased stiffness and
14
15 7 anisotropy is likely the stretching of collagen-based structures within the muscle, including
16
17 8 epimysium, perimysium, and endomysium as well as the muscle fiber extracellular matrix,
18
19 9 resulting in higher levels of pre-stress and pre-strain within the tissue [63]. As these collagen
20
21 10 structures are stretched, the collagen becomes more highly aligned [64,65], which has also
22
23 11 been reflected in diffusion imaging studies [15,17]. The pathway for the increase in tension is
24
25 12 likely also related to titin, the third structural protein within sarcomeres which studies suggest
26
27 13 causes passive force enhancement [66,67]. Titin primarily acts as a molecular spring with the
28
29 14 ability to alter stiffness during muscle activation to maintain stability in muscles that are
30
31 15 stretched to long lengths. Previous ex-vivo studies have also shown that muscle fibers and their
32
33 16 sarcomeres produce low levels of lateral forces during muscle lengthening [45,48], though in
34
35 17 this work we observed no significant change in μ_2 during passive muscle lengthening,
36
37 18 suggesting that the mechanism of lateral force creation may not be significant enough to be
38
39 19 detected via changes in substrate stiffness.

40
41 20 In a previous MRE study of skeletal muscle, Babaei et al. [37] found a similar relationship
42
43 21 between μ_1 and muscle length, though results differed for μ_2 and ϕ , as μ_2 significantly
44
45 22 increased while ϕ stayed relatively stable as the muscle stretched. One possible reason for
46
47
48
49
50
51
52
53
54
55
56
57
58
59
60

1 differences in these results is the different material models used in the two studies. Babei, et al.
2 assumed tissue incompressibility with only the presence of slow propagating shear waves, and
3 accordingly, no fast propagating shear wave effects (i.e. only shear anisotropy and no tensile
4 anisotropy). Ignoring the fast shear wave component in skeletal muscle may bias estimates of
5 shear moduli, since fast waves are likely to be present in an NITI material unless care is taken to
6 avoid their excitation [39]. Under the assumption of full incompressibility, tissue stretching
7 must be represented in other measurements, possibly resulting in the mismatch in outcomes
8 between the two studies. Another possible explanation could be the lack of knee restraint in
9 the Babei study. As previously noted, the gastrocnemius muscle can be stretched or shortened
10 by changing the angle of either the ankle or knee; hence, while the ankle angle was controlled,
11 any readjustment of the subject's knee angle will cause changes in length and pennation angle
12 of the muscle, and potentially change the resulting material property parameter estimates.

13 In Experiment 2, we demonstrated the effects of isometric contraction on the
14 anisotropic material properties of the gastrocnemius. Results from this experiment indicate
15 that as this activation occurs, the muscle increases its shear stiffness in the direction
16 perpendicular to the fiber direction. Previous studies utilizing MRE for estimation of skeletal
17 muscle during activation, such as works by Zonnino, et al. [31] and Schrank, et al. [32], also
18 reported increases in stiffness estimates during isometric contractions. These studies also
19 found greater increases during agonist actions than antagonist actions, with the gastrocnemius
20 functioning as an agonist during plantar-flexion, displaying larger parameter changes than in
21 dorsi-flexion, or antagonist action for the gastrocnemius. Our TI-NLI anisotropic property
22 estimates suggest the increase in stiffness estimated in these previous studies was a result of

1 stiffening of the tissue in the perpendicular direction with little to no increase in stiffness in the
2 fiber direction during activation. We expect these increases during isometric contraction are a
3 consequence of the cross-bridge model attributed to Huxley, et al. [68], which indicates that
4 cross-bridges are created by myosin and actin bonding, which exert forces along the bridge
5 during bonding that occurs in conjunction with conversion of ATP into ADP. This cross-bridge
6 loading creates lateral stresses between sarcomeres, specifically the z-disc, the region of the
7 muscle fiber linking sarcomeres together, and upon the surrounding collagen supportive
8 structures [46,47]. However, the forces are not a constant, as the cross-bridge only spends a
9 portion of time strongly attached to actin. The amount of time these cross-bridges spend
10 attached to actin fibrils increases in response to load. Thus, the cross-bridge “duty cycle” is high
11 frequency, meaning that MRE likely captures an averaged state of the cross-bridge loading and
12 unloading [67,69].

13 The two experiments reported here highlight how anisotropic MRE utilizing TI-NLI can
14 be an effective tool for *in-vivo* mechanical evaluation of skeletal muscle structural and
15 functional health and agree with mechanical responses of muscle shown in previous *ex-vivo*
16 experiments. First, we observed how shear stiffness parallel and perpendicular to muscle
17 fibers, μ_1 and μ_2 , influenced the complex relationship between ϕ and muscle loading. μ_1
18 correlates with increasing tension caused by muscle lengthening through passive loading, while
19 μ_2 captures the lateral loading across cross-bridges and between sarcomeres and the
20 surrounding collagen-based structures that occurs during isometric contraction. On the other
21 hand, while ζ appears to be a necessary component of the parameter estimation process and
22 shows changes with both passive lengthening and active contraction, ζ is the most common

1 anisotropic material parameter explored in previous *ex-vivo* experiments. While the responses
2 of ζ are similar to those of ϕ in these experiments, differences between the two parameters in
3 future experiments could help provide greater insight into tissue behavior.

4 Muscle under tension not only changes the shape and structure of cells, which are
5 expected to affect tissue mechanics, but also generates significant pre-strain fields which
6 further influence shear wave propagation. Muscle stress fields can be reasonably approximated
7 as having symmetry around an axis along the length of the muscle, so these effects can be
8 adequately modeled by effective parameters of a NITI model [49]. A simple model of passive
9 stretching produces tensile pre-stress fields along the muscle, and radially symmetric
10 compressive pre-stress perpendicular to the muscle axis due to the Poisson effect [70]. This will
11 increase shear wave speed along the muscle axis and perpendicular to the muscle axis, though
12 likely a lesser amount, resulting in an increased apparent anisotropy. Active muscle contraction
13 also has tensile stress along the muscle axis; however, this is generated by shortening the
14 muscle which increases cross-sectional area which gives a tensile pre-strain. This increases
15 wave speed in both directions, giving an increased overall effective stiffness, and lower
16 effective anisotropy. Accurate modeling of these acoustoelastic effects [54,71,72] requires a
17 nonlinear computational model and knowledge of the both the pre-strain field, requiring the
18 unstressed state to be known, and the nonlinear mechanical properties. As these requirements
19 are difficult to achieve with *in-vivo* imaging, separation of the mechanical property changes
20 from acoustoelastic changes is not currently feasible. Therefore, a small displacement
21 assumption is used in the estimation of “effective” mechanical properties which consist of the
22 true unstressed properties mixed with the nonlinear acoustoelastic effects from the pre-strain

1 field. These effective properties are altered by both changes in cellular structure and changes in
2 muscle function, so provided conditions are controlled carefully they can provide useful insight
3 into muscle health.

4 While the methods utilized in this study were effective at capturing the viscoelastic
5 responses of muscle function with MRE, the study had several limitations. While the MRE and
6 DTI scans have standard imaging noise, other biological tissues and structures within the
7 volume create additional noise and discontinuities that may affect outcomes [73]. These
8 structures include the fibula, major blood vessels, fatty tissue, and muscle fascia, each of which
9 create challenges for MRE, as they introduce model-data mismatch in multiple small ROIs that
10 we sought to minimize by incorporating spatial information in the inversion process. Muscle
11 fatigue also potentially affected outcomes from Experiment 2 that required consistent force
12 generation over a period of time [74,75]. Experiment 2 was designed using springs that
13 generate a load below 15% mean voluntary contraction for an average human adult, to avoid
14 significant fatigue during the short imaging time, but this threshold is variable from subject to
15 subject and levels of force application were imprecise as no *in-situ* measurements were
16 recorded. One additional limitation is possible differences in assumed fiber direction for
17 anisotropic estimation and the true fiber direction, especially during Experiment 2, as DTI data
18 was not acquired during each isometric contraction condition but rather was acquired at rest
19 and registered to MRE data from active contraction prior to TI-NLI. Recommendations for
20 future studies include a tailored force output requirement based on an individual subject's MVC
21 and a visual feedback system adjusted to each subject's necessary output level so that a
22 participant can maintain the proper level of contraction. Additionally, subject knee and ankle

1 positions in both experiments were relatively well controlled and consistent within an
2 individual subject's data set, however they were unmeasured and could not be accounted for
3 during statistical analysis, and differences between individuals may account for some of the
4 variability in observed outcomes.

5 **5. Conclusions**

6 In this work, we use anisotropic MRE to capture functional effects on muscle mechanics,
7 including passive muscle lengthening and active contraction to the medial and lateral heads of
8 the gastrocnemius. Using TI-NLI, we generated anisotropic material parameter maps and
9 estimated each parameter within the muscle volumes of participants for each of three
10 conditions during each experiment capturing both passive lengthening and active contraction.
11 Anisotropic mechanical parameters exhibited different trends based on the loading condition,
12 and MRE with TI-NLI may allow us to examine healthy functional response of muscle tissue as
13 well as tissue affect by injuries or pathologies, such as cerebral palsy.

14 **6. Acknowledgements**

15 This study was supported in part by grants from the National Institutes of Health (R01-
16 EB027577) and the National Science Foundation (CBET-1911683).

18 **7. Ethical Statement**

19 This work with subjects was approved by the University of Delaware Institutional Review
20 Board with protocol number 1730839-1. All work was conducted in accordance with the
21 principles embodied in the Declaration of Helsinki and local requirements. Subjects gave
22 written informed consent to participate in the study and for publication.

1
2
3 1
4
5
6 2
7
8 3
9
10 4
11
12
13 5
14
15 6
16
17 7
18
19 8
20
21 9
22
23 10
24
25 11
26
27 12
28
29 13
30
31 14
32
33 15
34
35 16
36
37 17
38
39 18
40
41 19
42
43 20
44
45 21
46
47 22
48
49
50
51
52
53
54
55
56
57
58
59
60

8. Conflict of Interest

The authors have no conflicts of interest to disclose.

9. Bibliography

- [1] Raiteri, B. J., Hug, F., Cresswell, A. G., and Lichtwark, G. A., 2016, "Quantification of Muscle Co-Contraction Using Supersonic Shear Wave Imaging," *J. Biomech.*, **49**(3), pp. 493–495.
- [2] Komi, P. V., and Viitasalo, J. H. T., 1976, "Signal Characteristics of EMG at Different Levels of Muscle Tension," *Acta Physiol. Scand.*, **96**(2), pp. 267–276.
- [3] Kellis, E., and Baltzopoulos, V., 1998, "Muscle Activation Differences between Eccentric and Concentric Isokinetic Exercise.," *Med. Sci. Sports Exerc.*, **30**(11), pp. 1616–23.
- [4] Pillen, S., and van Alfen, N., 2011, "Skeletal Muscle Ultrasound," *Neurol. Res.*, **33**(10), pp. 1016–1024.
- [5] van Hooren, B., Teratsias, P., and Hodson-Tole, E. F., 2020, "Ultrasound Imaging to Assess Skeletal Muscle Architecture during Movements: A Systematic Review of Methods, Reliability, and Challenges," *J. Appl. Physiol.*, **128**(4), pp. 978–999.
- [6] Naruse, M., Trappe, S., and Trappe, T. A., 2022, "Human Skeletal Muscle Size with Ultrasound Imaging: A Comprehensive Review," *J. Appl. Physiol.*, **132**(5), pp. 1267–1279.
- [7] Díaz-Manera, J., Llauger, J., Gallardo, E., and Illa, I., 2015, "Muscle MRI in Muscular Dystrophies," *Acta Myol.*, **34**(2–3), p. 95.
- [8] Murphy, W. A., Totty, W. G., and Carroll, J. E., 1986, "MRI of Normal and Pathologic

- 1
2
3 1 Skeletal Muscle,” *Am. J. Roentgenol.*, **146**(3), pp. 565–574.
- 4
5
6 2 [9] Marty, B., and Carlier, P. G., 2019, “Physiological and Pathological Skeletal Muscle T1
7
8 3 Changes Quantified Using a Fast Inversion-Recovery Radial NMR Imaging Sequence,” *Sci.*
9
10 4 *Rep.*, **9**(1).
- 11
12
13 5 [10] Kalia, V., Leung, D. G., Sneag, D. B., Grande, F. Del, and Carrino, J. A., 2017, “Advanced
14
15 6 MRI Techniques for Muscle Imaging,” *Semin. Musculoskelet. Radiol.*, **21**(4), p. 459.
- 16
17
18 7 [11] Shen, W., Gong, X., Weiss, J., and Jin, Y., 2013, “Comparison among T1-Weighted
19
20 8 Magnetic Resonance Imaging, Modified Dixon Method, and Magnetic Resonance
21
22 9 Spectroscopy in Measuring Bone Marrow Fat,” *J. Obes.*, **2013**.
- 23
24
25 10 [12] Yao, L., Yip, A. L., Shrader, J. A., Mesdaghinia, S., Volochayev, R., Jansen, A. V., Miller, F.
26
27 11 W., and Rider, L. G., 2016, “Magnetic Resonance Measurement of Muscle T2, Fat-
28
29 12 Corrected T2 and Fat Fraction in the Assessment of Idiopathic Inflammatory
30
31 13 Myopathies,” *Rheumatology (Oxford)*, **55**(3), p. 441.
- 32
33
34
35 14 [13] Biglands, J. D., Grainger, A. J., Robinson, P., Tanner, S. F., Tan, A. L., Feiweier, T., Evans, R.,
36
37 15 Emery, P., and O’Connor, P., 2020, “MRI in Acute Muscle Tears in Athletes: Can
38
39 16 Quantitative T2 and DTI Predict Return to Play Better than Visual Assessment?,” *Eur.*
40
41 17 *Radiol.*, **30**(12), pp. 6603–6613.
- 42
43
44
45 18 [14] Johnston, J. H., Kim, H. K., Merrow, A. C., Laor, T., Serai, S., Horn, P. S., Kim, D. H., and
46
47 19 Wong, B. L., 2015, “Quantitative Skeletal Muscle MRI: Part 1, Derived T2 Fat Map in
48
49 20 Differentiation Between Boys With Duchenne Muscular Dystrophy and Healthy Boys,”
50
51 21 *Am. J. Roentgenol.*, **205**(2), pp. W207–W215.
- 52
53
54 22 [15] Schwenger, N. F., Steidle, G., Martirosian, P., Schraml, C., Springer, F., Claussen, C. D., and
55
56
57
58
59
60

- 1 Schick, F., 2009, "Diffusion Tensor Imaging of the Human Calf Muscle: Distinct Changes in
2 Fractional Anisotropy and Mean Diffusion Due to Passive Muscle Shortening and
3 Stretching," *NMR Biomed.*, **22**(10), p. 1047-1053.
- 4 [16] Sinha, S., Sinha, U., and Edgerton, V. R., 2006, "In Vivo Diffusion Tensor Imaging of the
5 Human Calf Muscle," *J. Magn. Reson. Imaging*, **24**(1), pp. 182–190.
- 6 [17] Oudeman, J., Nederveen, A. J., Strijkers, G. J., Maas, M., Luijten, P. R., and Froeling, M.,
7 2016, "Techniques and Applications of Skeletal Muscle Diffusion Tensor Imaging: A
8 Review," *J. Magn. Reson. Imaging*, **43**(4), pp. 773–788.
- 9 [18] Boesch, C., Slotboom, J., Hoppeler, H., and Kreis, R., 1997, "In Vivo Determination of
10 Intra-Myocellular Lipids in Human Muscle by Means of Localized ¹H-MR-Spectroscopy,"
11 *Magn. Reson. Med.*, **37**(4), pp. 484–493.
- 12 [19] Deshmukh, S., Subhawong, T., Carrino, J. A., and Fayad, L., 2014, "Role of MR
13 Spectroscopy in Musculoskeletal Imaging," *Indian J. Radiol. Imaging*, **24**(3), p. 210.
- 14 [20] Hiscox, L. V, Johnson, C. L., Barnhill, E., McGarry, M. D. J., Huston, J., van Beek, E. J. R.,
15 Starr, J. M., and Roberts, N., 2016, "Magnetic Resonance Elastography (MRE) of the
16 Human Brain: Technique, Findings and Clinical Applications," *Phys. Med. Biol.*, **61**(24), pp.
17 R401–R437.
- 18 [21] Bayly, P. V., and Garbow, J. R., 2018, "Pre-Clinical MR Elastography: Principles,
19 Techniques, and Applications," *J. Magn. Reson.*, **291**, pp. 73–83.
- 20 [22] Mariappan, Y. K., Glaser, K. J., and Ehman, R. L., 2010, "Magnetic Resonance
21 Elastography: A Review," *Clin. Anat.*, **23**(5), pp. 497–511.
- 22 [23] Litwiller, D. V, Mariappan, Y. K., and Ehman, R. L., 2012, "Magnetic Resonance

- 1
2
3 1 Elastography,” *Curr. Med. Imaging Rev.*, **8**(1), pp. 46–55.
- 4
5
6 2 [24] Debernard, L., Robert, L., Charleux, F., and Bensamoun, S. F., 2011, “Characterization of
7
8 3 Muscle Architecture in Children and Adults Using Magnetic Resonance Elastography and
9
10 4 Ultrasound Techniques,” *J. Biomech.*, **44**(3), pp. 397–401.
- 11
12
13 5 [25] Kennedy, P., Barnhill, E., Gray, C., Brown, C., van Beek, E. J. R., Roberts, N., and Greig, C.
14
15 6 A., 2020, “Magnetic Resonance Elastography (MRE) Shows Significant Reduction of Thigh
16
17 7 Muscle Stiffness in Healthy Older Adults,” *GeroScience*, **42**(1), pp. 311–321.
- 18
19
20 8 [26] Green, M. A., Sinkus, R., Gandevia, S. C., Herbert, R. D., and Bilston, L. E., 2012,
21
22 9 “Measuring Changes in Muscle Stiffness after Eccentric Exercise Using Elastography,”
23
24 10 *NMR Biomed.*, **25**(6), pp. 852–858.
- 25
26
27 11 [27] Kennedy, P., Macgregor, L. J., Barnhill, E., Johnson, C. L., Perrins, M., Hunter, A., Brown,
28
29 12 C., van Beek, E. J. R., and Roberts, N., 2017, “MR Elastography Measurement of the Effect
30
31 13 of Passive Warmup Prior to Eccentric Exercise on Thigh Muscle Mechanical Properties,” *J.*
32
33 14 *Magn. Reson. Imaging*, **46**(4), pp. 1115–1127.
- 34
35
36 15 [28] Basford, J. R., Jenkyn, T. R., An, K.-N., Ehman, R. L., Heers, G., and Kaufman, K. R., 2002,
37
38 16 “Evaluation of Healthy and Diseased Muscle with Magnetic Resonance Elastography,”
39
40 17 *Arch. Phys. Med. Rehabil.*, **83**(11), pp. 1530–1536.
- 41
42
43 18 [29] Ringleb, S. I., Bensamoun, S. F., Chen, Q., Manduca, A., An, K.-N., and Ehman, R. L., 2007,
44
45 19 “Applications of Magnetic Resonance Elastography to Healthy and Pathologic Skeletal
46
47 20 Muscle,” *J. Magn. Reson. Imaging*, **25**(2), pp. 301–9.
- 48
49
50 21 [30] Bensamoun, S. F., Charleux, F., Debernard, L., Themar-Noel, C., and Voit, T., 2015, “Elastic
51
52 22 Properties of Skeletal Muscle and Subcutaneous Tissues in Duchenne Muscular
53
54
55
56
57
58
59
60

- 1
2
3 1 Dystrophy by Magnetic Resonance Elastography (MRE): A Feasibility Study,” *IRBM*, **36**(1),
4
5
6 2 pp. 4–9.
7
8 3 [31] Zonnino, A., Smith, D. R., Delgorio, P. L., Johnson, C. L., and Sergi, F., 2019, “MM-MRE: A
9
10 4 New Technique to Quantify Individual Muscle Forces during Isometric Tasks of the Wrist
11
12 5 Using MR Elastography,” *IEEE Int. Conf. Rehabil. Robot.*, **2019-June**, pp. 270–275.
13
14
15 6 [32] Schrank, F., Warmuth, C., Görner, S., Meyer, T., Tzschätzsch, H., Guo, J., Uca, Y. O., Elgeti,
16
17 7 T., Braun, J., and Sack, I., 2020, “Real-Time MR Elastography for Viscoelasticity
18
19 8 Quantification in Skeletal Muscle during Dynamic Exercises,” *Magn. Reson. Med.*, **84**(1),
20
21 9 pp. 103–114.
22
23
24 10 [33] Palnitkar, H., Reiter, R. O., Majumdar, S., Lewis, P., Hammersley, M., Shah, R. N., Royston,
25
26 11 T. J., and Klatt, D., 2019, “An Investigation into the Relationship between Inhomogeneity
27
28 12 and Wave Shapes in Phantoms and Ex Vivo Skeletal Muscle Using Magnetic Resonance
29
30 13 Elastography and Finite Element Analysis,” *J. Mech. Behav. Biomed. Mater.*, **98**, pp. 108–
31
32 14 120.
33
34
35 15 [34] Guidetti, M., Lorgna, G., Klatt, D., Vena, P., and Royston, T. J., 2019, “Anisotropic
36
37 16 Composite Material Phantom to Improve Skeletal Muscle Characterization Using
38
39 17 Magnetic Resonance Elastography,” *J. Mech. Behav. Biomed. Mater.*, **89**, pp. 199–208.
40
41
42 18 [35] Green, M. A., Geng, G., Qin, E., Sinkus, R., Gandevia, S. C., and Bilston, L. E., 2013,
43
44 19 “Measuring Anisotropic Muscle Stiffness Properties Using Elastography,” *NMR Biomed.*,
45
46 20 **26**(11), pp. 1387–1394.
47
48
49 21 [36] Guo, J., Hirsch, S., Scheel, M., Braun, J., and Sack, I., 2016, “Three-Parameter Shear Wave
50
51 22 Inversion in MR Elastography of Incompressible Transverse Isotropic Media: Application
52
53
54
55
56
57
58
59
60

- 1
2
3 1 to in Vivo Lower Leg Muscles,” *Magn. Reson. Med.*, **75**(4), pp. 1537–1545.
- 4
5
6 2 [37] Babaei, B., Fovargue, D., Lloyd, R. A., Miller, R., Jugé, L., Kaplan, M., Sinkus, R.,
7
8 3 Nordsletten, D. A., and Bilston, L. E., 2021, “Magnetic Resonance Elastography
9
10 4 Reconstruction for Anisotropic Tissues,” *Med. Image Anal.*, **74**.
- 11
12
13 5 [38] Feng, Y., Okamoto, R. J., Namani, R., Genin, G. M., and Bayly, P. V., 2013, “Measurements
14
15 6 of Mechanical Anisotropy in Brain Tissue and Implications for Transversely Isotropic
16
17 7 Material Models of White Matter,” *J. Mech. Behav. Biomed. Mater.*, **23**, pp. 117–132.
- 18
19
20 8 [39] Tweten, D. J. D. J., Okamoto, R. J., Schmidt, J. L., Garbow, J. R., and Bayly, P. V., 2015,
21
22 9 “Estimation of Material Parameters from Slow and Fast Shear Waves in an
23
24 10 Incompressible, Transversely Isotropic Material,” *J. Biomech.*, **48**(15), pp. 4002–4009.
- 25
26
27 11 [40] Tweten, D. J., Okamoto, R. J., and Bayly, P. V., 2017, “Requirements for Accurate
28
29 12 Estimation of Anisotropic Material Parameters by Magnetic Resonance Elastography: A
30
31 13 Computational Study,” *Magn. Reson. Med.*, **78**(6), pp. 2360–2372.
- 32
33
34 14 [41] Smith, D. R., Guertler, C. A., Okamoto, R. J., Romano, A. J., Bayly, P. V., and Johnson, C. L.,
35
36 15 2020, “Multi-Excitation Magnetic Resonance Elastography of the Brain: Wave
37
38 16 Propagation in Anisotropic White Matter,” *J. Biomech. Eng.*, **142**(7), pp. 51–59.
- 39
40
41 17 [42] Smith, D. R., Caban-Rivera, D. A., McGarry, M. D. J., Williams, L. T., McIlvain, G., Okamoto,
42
43 18 R. J., Van Houten, E. E. W., Bayly, P. V., Paulsen, K. D., and Johnson, C. L., 2022,
44
45 19 “Anisotropic Mechanical Properties in the Healthy Human Brain Estimated with Multi-
46
47 20 Excitation Transversely Isotropic MR Elastography,” *Brain Multiphysics*, **3**, p. 100051.
- 48
49
50 21 [43] Huijing, P. A., 1999, “Muscle as a Collagen Fiber Reinforced Composite: A Review of Force
51
52 22 Transmission in Muscle and Whole Limb,” *J. Biomech.*, **32**(4), pp. 329–345.
- 53
54
55
56
57
58
59
60

- 1
2
3 1 [44] Wheatley, B. B., 2020, "Investigating Passive Muscle Mechanics With Biaxial Stretch,"
4
5 Front. Physiol., **11**, p. 1021.
6
7
8 3 [45] Mohammadkhah, M., Murphy, P., and Simms, C. K., 2018, "Collagen Fibril Organization in
9
10 Chicken and Porcine Skeletal Muscle Perimysium under Applied Tension and
11
12 Compression," J. Mech. Behav. Biomed. Mater., **77**, pp. 734–744.
13
14
15 6 [46] Ramaswamy, K. S., Palmer, M. L., Van Der Meulen, J. H., Renoux, A., Kostrominova, T. Y.,
16
17 Michele, D. E., Faulkner, J. A., Faulkner, J. A., and Michele, D. E., 2011, "Lateral
18
19 Transmission of Force Is Impaired in Skeletal Muscles of Dystrophic Mice and Very Old
20
21 Rats Corresponding Authors," J. Physiol. J Physiol, **589**(5), pp. 1195–1208.
22
23
24
25 10 [47] Maas, H., 2019, "Significance of Epimuscular Myofascial Force Transmission under
26
27 Passive Muscle Conditions," J. Appl. Physiol., **126**(5), pp. 1465–1473.
28
29
30 12 [48] Böl, M., 2009, "Micromechanical Modelling of Skeletal Muscles: From the Single Fibre to
31
32 the Whole Muscle," Arch. Appl. Mech. 2009 805, **80**(5), pp. 557–567.
33
34
35 14 [49] Takaza, M., Moerman, K. M., Gindre, J., Lyons, G., and Simms, C. K., 2013, "The
36
37 Anisotropic Mechanical Behaviour of Passive Skeletal Muscle Tissue Subjected to Large
38
39 Tensile Strain," J. Mech. Behav. Biomed. Mater., **17**, pp. 209–220.
40
41
42 17 [50] McGarry, M., Houten, E. Van, Guertler, C., Okamoto, R., Smith, D., Sowinski, D., Johnson,
43
44 C., Bayly, P., Weaver, J., and Paulsen, K., 2021, "A Heterogenous, Time Harmonic, Nearly
45
46 Incompressible Transverse Isotropic Finite Element Brain Simulation Platform for MR
47
48 Elastography," Phys. Med. Biol., **66**(5), p. 055029.
49
50
51
52 21 [51] McGarry, M., Van Houten, E., Sowinski, D., Jyoti, D., Smith, D. R., Caban-Rivera, D. A.,
53
54 McIlvain, G., Bayly, P., Johnson, C. L., Weaver, J., and Paulsen, K., 2022, "Mapping
55
56
57
58
59
60

- 1
2
3 1 Heterogenous Anisotropic Tissue Mechanical Properties with Transverse Isotropic
4
5
6 2 Nonlinear Inversion MR Elastography,” *Med. Image Anal.*, **78**, p. 102432.
7
8 [52] Jenkinson, M., Beckmann, C. F., Behrens, T. E. J. J., Woolrich, M. W., and Smith, S. M.,
9
10 2012, “Fsl,” *Neuroimage*, **62**(2), pp. 782–90.
11
12
13 [53] Jenkinson, M., 2003, “Fast, Automated, N-Dimensional Phase-Unwrapping Algorithm,”
14
15 6 *Magn. Reson. Med.*, **49**(1), pp. 193–197.
16
17
18 [54] Abiza, Z., Destrade, M., and Ogden, R. W., 2012, “Large Acoustoelastic Effect,” *Wave*
19
20 8 *Motion*, **49**(2), pp. 364–374.
21
22
23 [55] McGarry, M., Johnson, C. L., Sutton, B. P., Van Houten, E. E., Georgiadis, J. G., Weaver, J.
24
25 10 B., and Paulsen, K. D., 2013, “Including Spatial Information in Nonlinear Inversion MR
26
27 11 Elastography Using Soft Prior Regularization,” *IEEE Trans. Med. Imaging*, **32**(10), pp.
28
29 12 1901–1909.
30
31
32 [56] Johnson, C. L., McGarry, M. D. J., Gharibans, A. A., Weaver, J. B., Paulsen, K. D., Wang, H.,
33
34 14 Olivero, W. C., Sutton, B. P., and Georgiadis, J. G., 2013, “Local Mechanical Properties of
35
36 15 White Matter Structures in the Human Brain,” *Neuroimage*, **79**, pp. 145–152.
37
38
39 [57] McGarry, M. D. J., Van Houten, E. E. W., Sowinski, D., Jyoti, D., Smith, D., Caban-Rivera, D.
40
41 17 A., McIlvain, G., Bayly, P., Johnson, C. L., Weaver, J. B., and Paulsen, K., 2021, “Mapping
42
43 18 Heterogenous Anisotropic Tissue Mechanical Properties with Transverse Isotropic
44
45 19 Nonlinear Inversion MR Elastography.” "In Rev.
46
47
48
49 [58] Maganaris, C. N., 2003, “Force-Length Characteristics of the in Vivo Human
50
51 21 Gastrocnemius Muscle,” *Clin. Anat.*, **16**(3), pp. 215–223.
52
53
54 [59] Riemann, B. L., DeMont, R. G., Ryu, K., and Lephart, S. M., 2001, “The Effects of Sex, Joint
55
56
57
58
59
60

- 1
2
3 1 Angle, and the Gastrocnemius Muscle on Passive Ankle Joint Complex Stiffness,” *J. Athl.*
4
5
6 2 *Train.*, **36**(4), p. 369.
- 7
8 3 [60] Evans, C. L., and Hill, A. V., 1914, “The Relation of Length to Tension Development and
9
10 4 Heat Production on Contraction in Muscle,” *J. Physiol.*, **49**(1–2), pp. 10–16.
- 11
12
13 5 [61] Gordon, A. M., Huxley, A. F., and Julian, F. J., 1966, “The Variation in Isometric Tension
14
15 6 with Sarcomere Length in Vertebrate Muscle Fibres,” *J. Physiol.*, **184**(1), pp. 170–192.
- 16
17
18 7 [62] Kaufman, K. R., An, K. N., and Chao, E. Y. S., 1989, “Incorporation of Muscle Architecture
19
20 8 into the Muscle Length-Tension Relationship,” *J. Biomech.*, **22**(8–9), pp. 943–948.
- 21
22
23 9 [63] Stecco, C., Pirri, C., Fede, C., Yucesoy, C. A., De Caro, R., and Stecco, A., 2021, “Fascial or
24
25 10 Muscle Stretching? A Narrative Review,” *Appl. Sci.*, **11**(1), pp. 1–11.
- 26
27
28 11 [64] Csapo, R., Gumpenberger, M., and Wessner, B., 2020, “Skeletal Muscle Extracellular
29
30 12 Matrix – What Do We Know About Its Composition, Regulation, and Physiological Roles?
31
32 13 A Narrative Review,” *Front. Physiol.*, **11**, p. 253.
- 33
34
35 14 [65] Gillies, A. R., and Lieber, R. L., 2011, “Structure and Function of the Skeletal Muscle
36
37 15 Extracellular Matrix,” *Muscle Nerve*, **44**(3), pp. 318–331.
- 38
39
40 16 [66] Herzog, W., Duvall, M., and Leonard, T. R., 2012, “Molecular Mechanisms of Muscle
41
42 17 Force Regulation: A Role for Titin?,” *Exerc. Sport Sci. Rev.*, **40**(1), pp. 50–57.
- 43
44
45 18 [67] Herzog, W., Powers, K., Johnston, K., and Duvall, M., 2015, “A New Paradigm for Muscle
46
47 19 Contraction,” *Front. Physiol.*, **6**(MAY), p. 174.
- 48
49
50 20 [68] Huxley, A. F. ., 1957, “Muscle Structure and Theories of Contraction,” *Prog. Biophys.*
51
52 21 *Biophys. Chem.*, **7**, pp. 255–318.
- 53
54
55 22 [69] Huxley, A. F., and Simmons, R. M., 1971, “Proposed Mechanism of Force Generation in
56
57
58
59
60

- 1
2
3 1 Striated Muscle,” Nat. 1971 2335321, **233**(5321), pp. 533–538.
4
5
6 2 [70] Pietsch, R., Wheatley, B. B., Donahue, T. L. H., Gilbrech, R., Prabhu, R., Liao, J., and
7
8 3 Williams, L. N., 2014, “Anisotropic Compressive Properties of Passive Porcine Muscle
9
10 4 Tissue,” J. Biomech. Eng., **136**(11).
11
12
13 5 [71] Crutison, J., and Royston, · Thomas, 2022, “The Design and Application of a Diffusion
14
15 6 Tensor Informed Finite-Element Model for Exploration of Uniaxially Prestressed Muscle
16
17 7 Architecture in Magnetic Resonance Imaging,” Eng. with Comput. 2022, **1**, pp. 1–16.
18
19
20 8 [72] Crutison, J., Sun, M., and Royston, T. J., 2022, “The Combined Importance of Finite
21
22 9 Dimensions, Anisotropy, and Pre-Stress in Acoustoelastography,” J. Acoust. Soc. Am.,
23
24
25 10 **151**(4), p. 2403.
26
27
28 11 [73] McGarry, M. D. J., Van Houten, E. E. W., Perriñez, P. R., Pattison, A. J., Weaver, J. B., and
29
30 12 Paulsen, K. D., 2011, “An Octahedral Shear Strain-Based Measure of SNR for 3D MR
31
32 13 Elastography,” Phys. Med. Biol., **56**(13), pp. N153-64.
33
34
35 14 [74] Fitts, R. H., 2008, “The Cross-Bridge Cycle and Skeletal Muscle Fatigue,” J. Appl. Physiol.,
36
37 15 **104**(2), pp. 551–558.
38
39
40 16 [75] McLester, J. R., 2012, “Muscle Contraction and Fatigue,” Sport. Med., **23**(5), pp. 287–305.
41
42
43
44
45
46
47
48
49
50
51
52
53
54
55
56
57
58
59
60